



HAL
open science

Biological sources and sinks of dimethylsulfide disentangled by an induced bloom experiment and a numerical model

Guillaume Le Gland, Marta Masdeu-Navarro, Martí Galí, Sergio M Vallina, Matti Gralka, Flora Vincent, Otto Cordero, Assaf Vardi, Rafel Simó

► **To cite this version:**

Guillaume Le Gland, Marta Masdeu-Navarro, Martí Galí, Sergio M Vallina, Matti Gralka, et al.. Biological sources and sinks of dimethylsulfide disentangled by an induced bloom experiment and a numerical model. *Limnology and Oceanography*, 2023, 10.1002/lno.12470 . hal-04361414

HAL Id: hal-04361414

<https://hal.science/hal-04361414>

Submitted on 28 Dec 2023

HAL is a multi-disciplinary open access archive for the deposit and dissemination of scientific research documents, whether they are published or not. The documents may come from teaching and research institutions in France or abroad, or from public or private research centers.

L'archive ouverte pluridisciplinaire **HAL**, est destinée au dépôt et à la diffusion de documents scientifiques de niveau recherche, publiés ou non, émanant des établissements d'enseignement et de recherche français ou étrangers, des laboratoires publics ou privés.

Biological sources and sinks of dimethylsulfide disentangled by an induced bloom experiment and a numerical model

Guillaume Le Gland ^{1,2*} Marta Masdeu-Navarro,¹ Martí Galí,¹ Sergio M. Vallina,³ Matti Gralka,^{4,5} Flora Vincent,^{6,7} Otto Cordero,⁴ Assaf Vardi,⁶ Rafel Simó ^{1*}

¹Department of Marine Biology and Oceanography, Institute of Marine Sciences (ICM—CSIC), Barcelona, Spain

²Mediterranean Institute of Oceanography (UMR 7294), Aix-Marseille Université, Université de Toulon, CNRS, IRD, Marseille, France

³Gijón Oceanography Centre, Spanish Institute of Oceanography (IEO—CSIC), Gijón, Spain

⁴Department of Civil and Environmental Engineering, Massachusetts Institute of Technology, Cambridge, Massachusetts, USA

⁵Systems Biology Lab, Amsterdam Institute for Life and Environment (A-LIFE), Vrije Universiteit Amsterdam, Amsterdam, The Netherlands

⁶Department of Plant and Environmental Sciences, Weizmann Institute of Science, Rehovot, Israel

⁷Developmental Biology Unit, EMBL, Heidelberg, Germany

Abstract

Dimethylsulfide (DMS) is a climatically active trace gas promoting cloud formation. The biochemical precursor of DMS, dimethylsulfoniopropionate (DMSP), is a phytoplankton metabolite and a source of reduced sulfur for many microbial species. Because of the complex interactions between their many producers and consumers, the dynamics of DMSP and DMS in the ocean are still poorly constrained. In this study we measure particulate DMSP, dissolved DMSP (DMSP_d), and DMS concentrations in seven mesocosms where two consecutive phytoplankton blooms (first, pico- and nano-algae; second, *Emiliania huxleyi*) were induced by nutrient addition, and we build a mechanistic numerical model to identify the sources and sinks that best account for the observations. The mesocosms were designed as replicates but differ from each other by their *E. huxleyi* virus abundance due to stochastic differences in initial conditions. The model shows that heterotrophic bacteria cannot be the only consumers of DMSP_d. A fraction of dissolved DMSP_d must be consumed by phytoplankton to avoid excessive DMSP_d accumulation during the first bloom. The induced blooms increase DMS concentration by 220% on average, until an increase in the abundance of DMS-consuming bacteria brings DMS concentration back to its pre-bloom value, after 3 weeks of experiment. Therefore phytoplankton blooms can increase DMS emission to the atmosphere, but only during a transient regime of a few weeks. The model also shows that the DMS yield, production and emission are increased when the coccolithophore bloom is terminated by a viral infection, but decreased if the infection occurs several days before the bloom can reach its maximum.

*Correspondence: guillaume.le-gland@univ-amu.fr; rsimo@icm.csic.es

This is an open access article under the terms of the [Creative Commons Attribution-NonCommercial-NoDerivs](https://creativecommons.org/licenses/by-nc-nd/4.0/) License, which permits use and distribution in any medium, provided the original work is properly cited, the use is non-commercial and no modifications or adaptations are made.

Additional Supporting Information may be found in the online version of this article.

Author Contribution Statement: G.L., M.M.-N., M.Ga., S.M.V., and R.S. conceived and designed the study. The induced bloom experiment was conducted by M.M.-N., F.V., O.C., A.V., and R.S. During this experiment, M.M.-N. and R.S. measured DMSP and DMS concentrations, and F.V. and A.V. measured phytoplankton and bacteria abundances. M.Gr. estimated the relative abundances of DMS-consuming bacteria by analyzing the 16S sequences under the supervision of O.C. G.L., M.Ga., S.M.V., and R.S. built the numerical model DMOS-BLOOM and analyzed its results. All authors contributed to and reviewed the manuscript.

Dimethylsulfide (DMS) is a climatically active trace gas that is found in the sunlit layer all over the world's ocean. Estimates of oceanic DMS emission to the atmosphere range from 17.6 to 34.4 Tg S yr⁻¹ (Kettle and Andreae 2000; Lana et al. 2011), with an average estimate of 27 Tg S yr⁻¹ (Hulswar et al. 2022). DMS emission and oxidation contribute to non-sea-salt sulfate and methanesulfonate production, and cloud condensation nuclei (CCN) formation (Charlson et al. 1987; Kulmala et al. 2014; Veres et al. 2020). The amount of atmospheric CCN impacts cloud albedo and therefore the Earth radiative budget (Twomey 1974). In this regard, a negative feedback between DMS production and Earth albedo has been postulated (Charlson et al. 1987), although this hypothesis is still debated to this day (Quinn and Bates 2011; Brévière et al. 2015; Wang et al. 2018).

The biochemical precursor of DMS, dimethylsulfoniopropionate (DMSP), is an important phytoplankton metabolite that plays a central role in the marine sulfur cycle. For instance, DMSP is a major source of sulfur for bacteria (Kiene et al. 1999). Although DMSP concentration in seawater is 6–7 orders of magnitude lower than that of sulfate, DMSP is taken up in preference to sulfate because it is already reduced and therefore requires less energy for incorporation into proteins. DMSP is of particular importance for the ubiquitous clade *SAR11* that does not have the genes to reduce inorganic sulfate (Tripp et al. 2008). Various studies identified DMSP either as an attractant across trophic levels of the planktonic food web (Miller et al. 2004; Seymour et al. 2010; Breckels et al. 2011) or on the contrary as a chemical defense deterring grazers (Wolfe et al. 1997; Strom et al. 2003). Among several known functions, DMSP has antioxidant properties (Sunda et al. 2002) and serves as an osmolyte in phytoplankton (Stefels 2000).

Intracellular DMSP, also called particulate DMSP (DMSP_p), is produced mainly by eukaryotic phytoplankton and released to the water as dissolved DMSP (DMSP_d) by cell death, including grazing by zooplankton and viral lysis. Living cells can also exude DMSP as an overflow mechanism for excess reduced sulfur or energy (Stefels 2000). The main sinks of DMSP_d are consumption by bacteria (Kiene et al. 1999; Simó et al. 2009) and phytoplankton (Vila-Costa et al. 2006a), including by some phytoplankton species that can produce their own DMSP (Spielmeyer et al. 2011). The majority of DMSP, usually around 90%, is consumed through the demethylation pathway, which allows for the incorporation of sulfur into methionine and does not produce DMS (Kiene and Linn 2000a; Moran et al. 2012; Galí and Simó 2015).

The remaining fraction of DMSP is cleaved into DMS and acrylate by enzymes collectively known as DMSP-lyases. Two types of organisms can cleave DMSP. Some eukaryotic phytoplankton species, like many haptophytes and dinoflagellates (Keller 1989; Alcolombri et al. 2015), possess DMSP lyases and can use them to produce DMS and remove excess carbon or scavenge harmful oxygen radicals (Vairavamurthy et al. 1985; Sunda et al. 2002; Stefels et al. 2007). Some DMSP-consuming bacteria also have DMSP-lyases and therefore cleave DMSP into DMS. Overall however, bacterial communities cleave only a fraction of the dissolved DMSP they consume into DMS, usually around 10% (Kiene and Linn 2000b). Bacterial DMSP cleavage is the main DMS source when the DMSP producers do not have DMSP lyase.

DMS is removed by both biotic and abiotic sinks. Some specialized bacteria, like *Methylophaga*, can consume DMS as their sole carbon source (Vila-Costa et al. 2006b; Schäfer 2007). A more common DMS degradation pathway in bacteria such as *Roseobacter* and the widespread *SAR11* is DMS oxidation to dimethylsulfoxide (DMSO) for energy gain in the presence of other carbon sources (Chen et al. 2011; Green et al. 2011; Hatton et al. 2012). In the uppermost, UV-exposed water

layer, DMS is degraded by photolysis (Toole et al. 2003; Galí et al. 2016). Finally, as a volatile, DMS is emitted to the atmosphere at a rate depending on wind speed, temperature, and DMS concentration (Kettle and Andreae 2000). Overall, DMS emission is a small sink, accounting for less than 10% of global DMS losses (Kloster et al. 2006; Galí and Simó 2015).

All the aforementioned sources and sinks are extremely variable in space and time, making any prediction of their response to future environmental changes challenging. The fluxes are affected by environmental parameters such as temperature, nutrient supply, and solar irradiance, both directly and through their impact on plankton community composition and ecophysiology. DMSP production varies by several orders of magnitude across phytoplankton taxa. For instance, haptophytes and dinoflagellates contain on average 10–30 times more DMSP per unit of biomass than diatoms, excluding the diatoms living in sea ice, whereas most cyanobacteria do not produce DMSP (Stefels et al. 2007). A large variability also exists within each group. In some phytoplankton species, high exposure to UV radiation (Archer et al. 2010) or low nutrient concentration (Bucciarelli and Sunda 2003; Harada et al. 2009; McParland and Levine 2019) has been shown to increase DMSP or DMS production. Both DMS producers and DMS consumers represent a variable minority fraction of heterotrophic bacteria. Therefore changes in the phytoplankton and heterotrophic bacteria community composition may have a larger impact on the production and consumption of DMSP and DMS than bulk biomass or primary production, with potential feedback on the food web and global climate.

The variability in the cycle of dimethylated sulfur compounds can be assessed through observations. Particulate and dissolved DMSP (Galí et al. 2015) and dissolved DMS (Hulswar et al. 2022) concentrations have been measured in situ at thousands of different locations of the surface ocean. The residence times and the relative contributions of each flux are more challenging to estimate and cannot be directly deduced from the concentrations. Indeed, a given concentration of DMS can be explained by a fast production and a fast removal, whereby the average residence time of a DMS molecule can be as short as a few hours, or by a slow production and a slow removal, with residence times of several days (Kiene and Linn 2000b). One way to estimate fluxes is to label DMS or DMSP with stable (e.g., ²H or ¹³C) or radioactive (e.g., ³⁵S) isotopes and track how these signature isotopes are transferred to other molecules over time (Kiene and Linn 2000a; Asher et al. 2011).

Mechanistic numerical modeling is another tool to estimate the fluxes that are not directly measured or sparsely so. Models transform the knowledge we have on processes into differential equations that can be solved by a computer. However, as our prior knowledge is incomplete, several sets of equations are possible. In addition, equations depend on parameters, some of which are poorly constrained. Yet, within the realistic range, some equations and parameter values account better than others for the observations, in our case the measured DMSP

and DMS concentrations, providing invaluable insight into the general rules controlling ecosystems.

In most global biogeochemistry models, like those used in coupled model intercomparison project exercises (Bock et al. 2021), DMS concentration is either a diagnostic function of chlorophyll, mixed layer depth, light or nutrients; or a tracer directly produced from DMSP_p by cell death and exudation. The dynamic model of oceanic sulfur (DMOS), developed in 2008 and dedicated to the cycle of organic sulfur in the Sargasso Sea (Vallina et al. 2008), is more comprehensive and reproduces the variations in DMSP_p, DMSP_d, and DMS concentrations over a year. DMOS resolved the role of seasonally varying abiotic factors, such as temperature, irradiance, and vertical mixing. In particular, Vallina et al. (2008) showed that the large DMS concentrations observed in summer could not be explained without allowing phytoplankton cells to leak DMS at high solar irradiance.

However, the aforementioned models only account for seasonal cycles and were not designed to explain how environmental factors changing at the timescale of a few days impact the fluxes of DMSP and DMS. During a phytoplankton bloom, temperature and day length are almost constant but nutrient concentrations and biotic factors, such as plankton biomass and species composition, vary rapidly (Levasseur et al. 2006). Measuring DMSP and DMS concentrations during a phytoplankton bloom is therefore ideal to discriminate the contribution of different species or different processes that would otherwise be difficult to separate, such as DMSP uptake by phytoplankton and DMSP uptake by heterotrophic bacteria.

In this work, we present new observations of DMSP and DMS concentrations and a new model to explain the sources and sinks of these two molecules. The model we built, called DMOS-Bloom, is a modified version of the DMOS model designed to reproduce DMSP_p, DMSP_d, and DMS concentrations during phytoplankton blooms. The data used to validate DMOS-Bloom were measured in a fjord and in seven mesocosms filled with fjord water and artificially enriched in nutrients. The mesocosms started from identical initial compositions but spontaneously diverged, most notably in the degree of viral infection of the main bloomer, the coccolithophore *Emiliania huxleyi*. With DMOS-Bloom, we investigate whether a model based on the current knowledge of dimethylated sulfur compounds cycling can reproduce the observed differences induced by nutrient concentration, taxonomic composition, and viral infection, and what the relative contribution of each source and sink is. The comparison of model and observations provides new insight into the impact of artificially induced phytoplankton blooms on DMS emission.

Materials and methods

Mesocosm experiments

All observations presented in this article come from an induced phytoplankton bloom experiment carried out between

the 23 May 2018 (day -1) and the 16 June 2018 (day 23) in Raunefjorden at the Marine Biological Station Espesgrend (60°16'11N; 5°13'07E) in southern Norway (Kuhlisch et al. 2021; Vincent et al. 2023). On day -1, seven light-transparent 4-m-deep enclosure bags were filled with nonfiltered surrounding fjord water and continuously mixed by air bubbling (from day 0 onward). On days 0–5 and 14–17, each bag was supplemented with nutrients (NaNO₃ and KH₂PO₄) at a nitrogen-to-phosphorus ratio of 16:1 (so that NO₃ concentration is increased by 1.6 μM per day and PO₄ is increased by 0.1 μM per day), whereas on days 6, 7, and 13, only nitrogen was added (Vincent et al. 2023). Water samples were collected daily (07:00 h) from each bag and from the surrounding fjord, which served as an environmental reference.

Nutrient concentrations and plankton abundances from each bag (Supplementary Figs. S1, S2) were measured by Vincent et al. (2023). In each bag, the phytoplankton community responded to nutrient addition (Supplementary Fig. S1a) with an increase in chlorophyll concentration compared to the surrounding fjord, and two consecutive phytoplankton blooms (Supplementary Fig. S1b) occurred. The first bloom, with a chlorophyll maximum on day 8 or 9 depending on the bag, was a bloom of a mixed algal community consisting mainly of picoeukaryote and nanoeukaryote (Supplementary Fig. S1c,d). The second bloom, with a chlorophyll maximum around day 18, was dominated by the coccolithophore *E. huxleyi* (Supplementary Fig. S1e).

Very similar dynamics were observed in bags 1, 2, 3, 5, and 6. In the validation process of DMOS-Bloom, we will treat them as replicates of the same experiment and compare their averaged results to a model simulation where the non-grazing mortality rate is constant and low. By contrast, bags 4 and 7 differed substantially from the other bags and from each other during the second half of the experiment. By far, they had the two largest abundances of *E. huxleyi* viruses, measured by quantitative polymerase chain reaction (Supplementary Fig. S1g); and the two largest proportions of infected *E. huxleyi* cells, measured by single-molecule fluorescence in situ hybridization (Supplementary Fig. S1h). Therefore bags 4 and 7 will be treated separately and compared with model simulations where the mortality rate of *E. huxleyi* is increased in order to account for the key role of viral lysis in the termination of the coccolithophore bloom.

DMSP and DMS measurements

DMS and DMSP were analyzed using a purge-and-trap system coupled to sulfur-specific gas chromatography (Shimadzu GC14A) with flame photometric detection. For DMS analysis immediately after sample collection, seawater aliquots of 2–5 mL were gently passed through a syringe filter (GF/F, Whatman) and immediately sparged in a crimp glass vial for 3–5 min with 40 mL min⁻¹ of high-purity helium (He). Volatiles were trapped in a 1/8" Teflon tube loop submerged in liquid nitrogen, from where they were revolatilized by dipping

the loop in water at room temperature. Sulfur compounds were separated using a packed Carboxpack 60/80 mesh column (Sigma-Aldrich) maintained at 170°C. Retention time for DMS was 0.9 min, and detection limit was 3 pmol. Analytical precision was better than 5%. Calibration was performed with a DMS standard solution prepared by alkaline hydrolysis of a DMSP solution in MilliQ water. Plots of $\log(\text{nmol DMS})$ vs. $\log(\text{peak area})$ yielded a straight line (usually $R^2 > 0.99$) that was used for DMS quantification in the samples. For dissolved DMSP (DMSP_d) analysis, 3 mL of seawater were gravity filtered through a 25-mm GF/F filter, and the filtrate was collected in a 10-mL glass vial. After addition of one NaOH pellet (45 mg, $\sim 0.1 \text{ mol L}^{-1}$ final concentration, $\text{pH} > 12$), the vial was crimped and stored overnight for alkaline DMSP hydrolysis. Evolved DMS was analyzed by purging the entire vial the same way as the samples above, and the DMSP_d concentration was calculated by subtraction of the corresponding, previously determined DMS concentration. For total DMSP (DMSP_t, i.e., dissolved + particulate) analysis, aliquots of 30 mL of unfiltered seawater were placed in gas-tight vials and hydrolyzed with two NaOH pellets. The DMSP_t + DMS was determined as evolved DMS after 4 months. To do so, small (10–500 μL) aliquots were withdrawn with a gas tight syringe and injected into the purge vial containing 2–4 mL of MilliQ water. Two DMSP_t + DMS samples were also run on-site 24 h after adding NaOH. The measurements of evolved DMS after 4 months were within 4% of the on-site measurements. The DMSP_t concentration was calculated by subtraction of the on-site determined DMS concentration. Particulate DMSP (DMSP_p) was calculated as $\text{DMSP}_t - \text{DMSP}_d$ with an uncertainty of 5%. The DMSP_p, DMSP_d, and DMS observations for each individual bag are available in Supplementary Fig. S3.

DMOS-Bloom step 1: Plankton ecosystem submodel

In order to simulate DMSP and DMS concentrations, DMOS-Bloom requires the biomass ($\mu\text{M-N}$) and the growth, mortality and grazing rates of all the microbes producing or consuming these two molecules. As these rates were not determined experimentally in the mesocosm experiment, they must be estimated by a model. Another limitation of the observed concentrations is that they oscillate, especially those of *E. huxleyi* (Fig. 1g), and there is no standard statistical method to tell what variability is real and what variability is due to measurement error. A mechanistic model provides a simple solution by fitting the part of variability that can be explained based on realistic estimates for growth and death and smoothing the part of variability that cannot be explained.

Therefore, the DMOS-Bloom model was designed to include a nitrogen-based phytoplankton ecosystem submodel (Fig. 1a) whose state variables, presented in Table 1a, are the concentrations of dissolved inorganic nitrogen (DIN) and organic nitrogen (ON) and the biomass of heterotrophic bacteria (*B*), four eukaryotic phytoplankton types (*P_i* with $1 \leq i \leq 4$) and five

zooplankton types (*Z_i* with $i \in \{1, 2, 3, 4, B\}$), one per prey type. To simplify the expression of the fluxes between the living (*B*, *P_i*, and *Z_i*) and the non-living (DIN and ON) nitrogen pools, the biomass of all microbes are expressed as molar concentrations of nitrogen. In the model, all phytoplankton types consume DIN, bacteria consume ON and each zooplankton type consumes only one prey type, either bacteria or one of the four phytoplankton types. We chose this food web for its simplicity and because it accounts well for the boom-and-bust dynamics experienced by each prey type (Supplementary Fig. S1c–f). The nitrogen cycle is closed when plankton mortality and a fraction of zooplankton grazing either goes to the organic nitrogen pool or is remineralized to DIN, immediately or through the action of bacteria. “Mortality” here and throughout the article refers to all non-grazing causes of cell death, including both background mortality and viral lysis. Heterotrophic bacteria are grouped in a single pool due to the lack of observations to separate the free-living and particle-attached fractions. As a consequence, organic nitrogen, the bacterial substrate, is not divided into dissolved and particulate fractions either. The four phytoplankton types represent eukaryotic picophytoplankton (type 1), two nanophytoplankton types (2 and 3), and calcified *E. huxleyi* (type 4), which also belongs to the nanophytoplankton size fraction but is treated separately due to its dominance during the second bloom. Nanophytoplankton are divided into two types because their overall biomass increases during both blooms but the species involved in each bloom are different (see fig. 2 of Vincent et al. (2023)). Eukaryotic picophytoplankton are grouped into a single type because their biomass increases only during the first bloom. The equations and parameters of the ecosystem submodel are presented in detail in the Supplementary Methods.

In order to explain the differences observed between the fjord and the seven bags, four virtual bags are simulated. The Control virtual bag simulates the fjord. The No-lysis virtual bag simulates bags 1, 2, 3, 5, and 6 and has an external nitrate input on days 0–7 and 13–17. The Late-lysis virtual bag simulates bag 4 and differs from the No-lysis virtual bag by imposing a higher mortality on nanophytoplankton and *E. huxleyi* and a higher bacterial growth rate from day 17 on. The Early-lysis virtual bag simulates bag 7 and is similar to the Late-lysis virtual bag but its mortality event starts earlier, on day 11. The differences between virtual bags and the corresponding mathematical parameterizations are described with more detail in Supplementary Table S1.

The comprehensive list of parameters shared by all virtual bags is presented in Supplementary Table S2 along with their values in DMOS-Bloom. Some parameters were set based on previous knowledge and others were optimized using a nonlinear least-squares method. The phytoplankton maximum growth rates estimated by optimization are all close to the prior estimate of 0.7 d^{-1} , which is very close to the nutrient replete growth rates measured in laboratories for species of

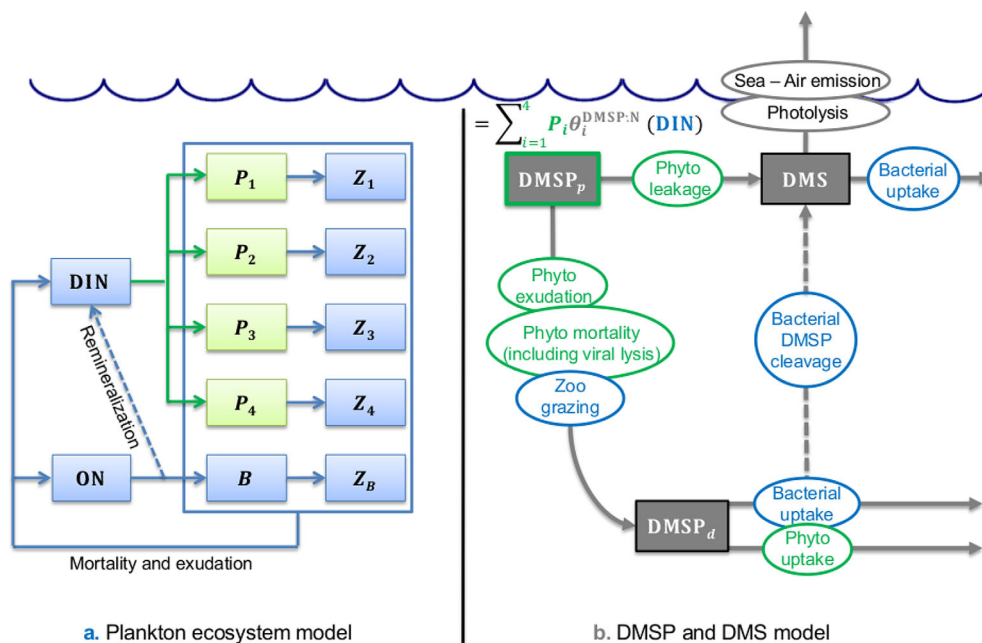


Fig. 1. Schematic diagram of the model. In the plankton ecosystem submodel (a), all stocks are in $\mu\text{M-N}$. P_i is the i^{th} phytoplankton species, Z_i is the i^{th} zooplankton species, DIN is dissolved inorganic nitrogen and ON is organic nitrogen, either particulate or dissolved. In the DMSP and DMS model (b), all stocks are in nM.

intermediate size (Marañon et al. 2013). As model plankton biomass is fitted to observations, the loss rate suffered by each prey type due to grazing and mortality is also expected to be realistic.

DMOS-Bloom step 2: DMSP and DMS submodel

The organic sulfur submodel (Fig. 1b) of DMOS-Bloom accounts for the production and removal of DMSP and DMS as a function of plankton biomass, reproduction, mortality and grazing rates, taken from the plankton ecosystem submodel. The parameters of the organic sulfur model are described in Supplementary Table S3. As the dynamics of organic sulfur are not precisely known, several scenarios, using different parameterizations for the sources and sinks, are tested and their results are compared to observations. The differences between the four scenarios are summarized in Table 2. All scenarios have dissolved DMSP (DMSP_d) and DMS as state variables, as shown in Table 1b. Scenario S4 has a third state variable which is the fraction $\chi^{(s)}$ of DMS-consuming specialists among bacteria. Particulate DMSP (DMSP_p) is not a state variable but is diagnosed at each time step based on phytoplankton biomass and DIN concentration.

Dissolved DMSP has three sources, all related to phytoplankton. When a phytoplankter suffers non-grazing mortality, 100% of its DMSP_p becomes dissolved. When it is grazed, a fraction $f = 70\%$ of its DMSP_p becomes dissolved and the remaining $1 - f = 30\%$ is assimilated by zooplankton and

Table 1. State variables of DMOS-Bloom. The four phytoplankton types are picophytoplankton ($i = 1$), first bloom nanophytoplankton ($i = 2$), second bloom nanophytoplankton ($i = 3$), and *Emiliania huxleyi* ($i = 4$).

(a) Ecosystem model		
Symbol	Description	Unit
$P_i \ i \in \{1,2,3,4\}$	Phytoplankton biomass (type i)	$\mu\text{M-N}$
B	Bacterial biomass	$\mu\text{M-N}$
$Z_i \ i \in \{1,2,3,4,B\}$	Zooplankton biomass (predator of type i)	$\mu\text{M-N}$
DIN	Dissolved inorganic nitrogen concentration	$\mu\text{M-N}$
ON	Organic nitrogen concentration	$\mu\text{M-N}$
(b) Organic sulfur model		
Symbol	Description	Unit
DMSP_d	Dissolved DMSP concentration	nM
DMS	DMS concentration	nM
χ_s	Fraction of specialist DMS-consuming bacteria	—

removed from the system (Simó 2004; Saló et al. 2009). The third source is phytoplankton DMSP exudation, which is proportional to DIN uptake and DMSP_p content. Dissolved DMSP has two sinks: consumption by picophytoplankton and by heterotrophic bacteria. DMS is produced in two different

Table 2. Model scenarios.

Process affecting S cycle	S1	S2	S3	S4
Phytoplankton DMSP : N ratio increase under nutrient stress	No	Yes	Yes	Yes
DMSP _d uptake by picophytoplankton	No	No	Yes	Yes
Variable fraction of DMS-consuming bacteria	No	No	No	Yes
Increased DMSP and DMS release during viral infection	No	No	No	Yes

ways: it is leaked by nanophytoplankton and *E. huxleyi* proportionally to their DIN uptake and DMSP_p content, and a fraction α (16–28%, depending on scenarios) of the DMSP_d consumed by heterotrophic bacteria is cleaved into DMS. DMS is then removed by two sinks: a constant abiotic sink ϕ (0.125 d⁻¹ in the fjord and 0.2 d⁻¹ in the mesocosms) and a variable consumption by heterotrophic bacteria. Bacterial DMS consumers are divided into generalists, which are a constant fraction of the bacterial biomass, and specialists, the fraction of which is constant in scenarios S1–S3 but variable in scenario S4.

Complexity is progressively increased from scenario S1–S4. Each scenario is designed to improve the ability of the model to reproduce one observed variable. From scenario S2 onward, the DMSP_p : N ratio of all phytoplankton types is higher under low nutrient concentration. Scenario S3 adds DMSP_d consumption by picophytoplankton to avoid DMSP_d accumulation when bacterial biomass is low. Finally, scenario S4 refines the dynamics of DMS by increasing DMS leakage by *E. huxleyi* cells during viral infections and allowing the fraction of specialist DMS-consuming bacteria to increase under high DMS concentration.

We define three additional diagnostic variables to further analyze the model outputs and allow comparisons with previous studies. The dissolved DMSP turnover rate constant (d⁻¹) is the ratio between DMSP_d removal and DMSP_d concentration. The turnover rate constant is high when the residence time (1 / [turnover rate constant], d) is low. The DMS turnover rate constant is defined in a similar way for DMS. The community DMS yield is the unitless ratio of DMS production to total DMSP consumption.

$$\begin{aligned} \text{DMSP}_d \text{ turnover} &= \frac{\text{DMSP}_d \text{ sink}}{\text{DMSP}_d \text{ concentration}} \\ &= \frac{\text{cons. by } B + \text{cons. by } P_1}{\text{DMSP}_d \text{ concentration}} \end{aligned} \quad (1)$$

$$\begin{aligned} \text{DMS turnover} &= \frac{\text{DMS sink}}{\text{DMS concentration}} \\ &= \phi + \frac{\text{cons. by gen. } B + \text{cons by spec. } B}{\text{DMS concentration}} \end{aligned} \quad (2)$$

$$\begin{aligned} \text{DMS yield} &= \frac{\text{DMS source}}{\text{DMSP}_{(d+p)} \text{ sink}} \\ &= \frac{\text{DMS leakage by } P_{2/3/4} + \text{DMSP}_d \text{ cleavage by } B}{\text{DMSP}_d \text{ cons. by } B/P_1 + \text{DMSP}_p \text{ assim. by } Z} \end{aligned} \quad (3)$$

Results

Model plankton and nutrient concentrations

The simulated microbial abundances and organic nitrogen concentrations of the No-lysis virtual bag fit very well with the corresponding observations (Fig. 2). All model concentrations are within the range of the corresponding observations, all mean errors (model – observations) are less than 10% of the mean observed concentrations and all linear correlations (R) between a model state variable and the corresponding set of observations from bags 1, 2, 3, 5, and 6 are between 0.8 and 1.

In both model and observations, picophytoplankton biomass (Fig. 2a) is close to 0.4 $\mu\text{M-N}$ at the beginning of the experiment, reaches a maximum of 3 $\mu\text{M-N}$ during the first bloom and then decreases continuously. From day 18 on, biomass is even lower than its initial observed and simulated value. The model explains the decline of picophytoplankton biomass after the first bloom and the subsequent lack of recovery by large grazing rates. The main mismatch between model and observations is that the initial picophytoplankton growth was faster in the observations, and a maximum was reached on day 6, i.e., 2 d earlier than in the model.

In both model and observations, nanophytoplankton biomass (Fig. 2b) exhibits two local maxima, one during each bloom. The amplitude of the second peak is slightly underestimated in the model, reaching 2.5 $\mu\text{M-N}$ instead of 3 $\mu\text{M-N}$. The first peak and the inter-bloom minimum have the same amplitude in model and observations but occurs 1 d earlier in the model.

Calcified *E. huxleyi* biomass (Fig. 2c) reached a maximum during the second bloom only. In observations, there were three consecutive peaks of *E. huxleyi* from day 17 to day 23 and biomass 2–4 times lower between the peaks. We do not know what process controls these oscillations. The growth rates that would be required to transition from a local minimum to a local maximum of biomass would be larger than 2 d⁻¹, which to our knowledge has never been observed for this species. The model is not able to reproduce the oscillations but has a maximum on day 18, which is the same time as in observations, and reproduces the average between peaks and troughs.

Bacterial biomass (Fig. 2d) is the model state variable that fits best with observations ($R = 0.95$ and mean error less than 2%) of mean observed biomass. The absolute maximum of bacterial biomass was reached on day 11, with 1.2 $\mu\text{M-N}$. Then bacterial biomass was reduced by two thirds, reaching a minimum on day 17 and then slightly increasing again until the

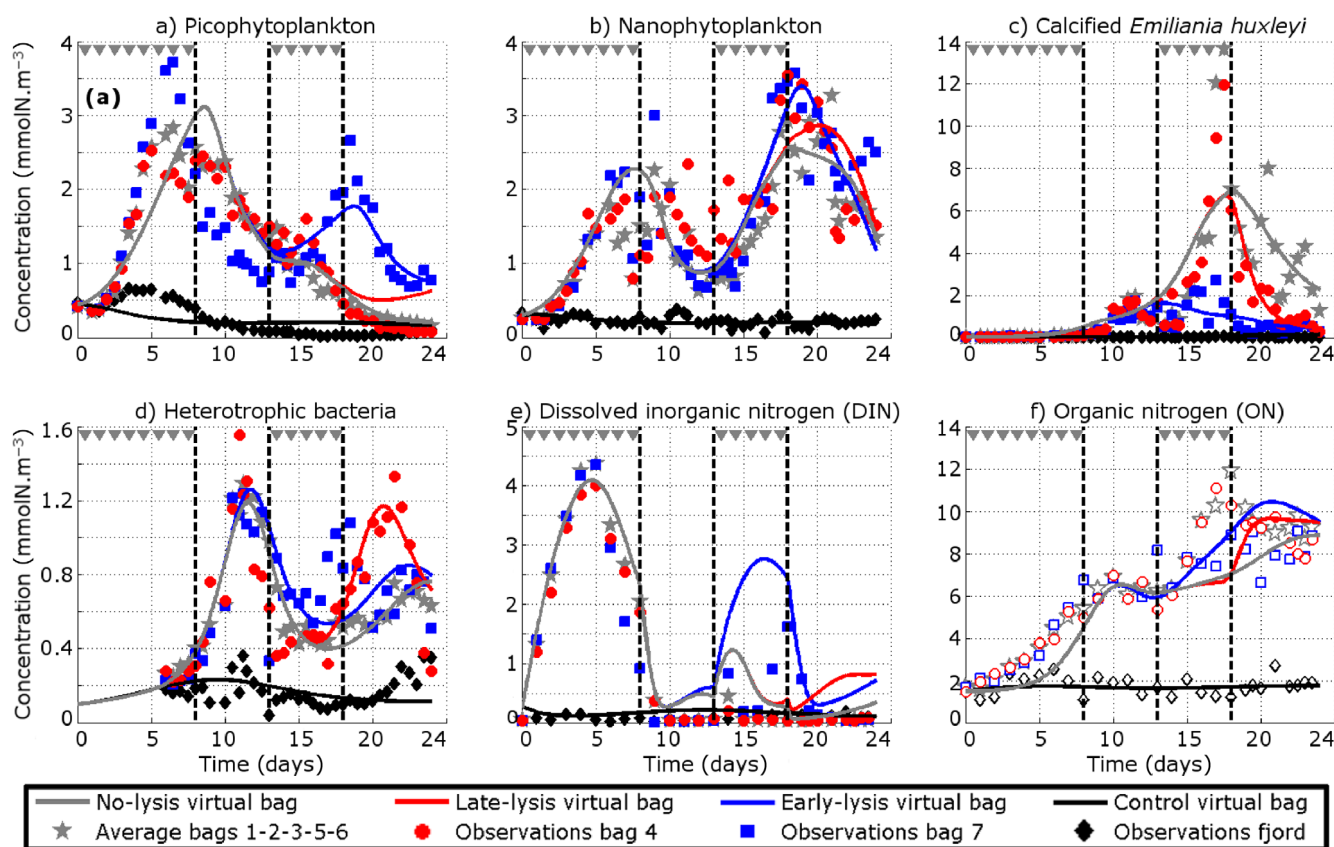


Fig. 2. Model plankton (a–d) and nutrient (e–f) outputs (lines) compared with observations (symbols). Lines and symbols represent model results and observations respectively. Each color represents a virtual bag and the observations it is designed to reproduce. Model organic nitrogen is compared with particulate organic nitrogen observations (open symbols) but these were not used to optimize the model parameters.

end of the experiment. In the model, the decrease after the absolute maximum is not due to a lack of organic matter, which is still very abundant, but to an increase in bacterivory.

Dissolved inorganic nitrogen (Fig. 2e) is compared to nitrate observations, knowing that nitrogen was the limiting nutrient and that the source of nitrogen added to the mesocosms to initiate phytoplankton blooms was nitrate. During the first bloom, modeled and observed nutrients coincide very precisely ($R = 0.98$ and mean error less than 2% of mean observed concentration). After day 9, nutrients are more abundant in the model, with an average of $0.4 \mu\text{M-N}$, than in the observations, with an average of $0.09 \mu\text{M-N}$. This difference was expected and is likely due to the presence of non-nitrate sources of inorganic nitrogen, such as ammonium and nitrite, which were not measured. The very low nitrate concentrations observed in the mesocosms would not be enough to sustain the phytoplankton biomass reached during the second bloom.

The ON pool of DMOS-Bloom represents the labile organic nitrogen, either dissolved or particulate, on which heterotrophic bacteria feed. Labile organic nitrogen has not been measured and the overall organic nitrogen stock is likely to be dominated by refractory organic matter (Benner and Amon 2015) that is irrelevant for our model. However, the

measured particulate organic nitrogen follows the same trend and order of magnitude as the model ON (Fig. 2f), increasing after each bloom from $1.5 \mu\text{M-N}$ at the beginning of the experiment to more than $8 \mu\text{M-N}$ at the end.

In fjord waters, the model results have the same order of magnitude as the observations but are more stable in time. Observations did not represent a steady state but oscillated, either as part of a seasonal cycle that was not measured or in response to a short term biotic or abiotic perturbation. These oscillations are out of the scope of the present study and are not precisely accounted for in the model.

From day 13 on, the Late-lysis and Early-lysis virtual bags differ from the No-lysis case. These differences have the same sign and occur at the same time as the observed differences between bags 4 or 7 and the average of the five other bags, and usually also have the same order of magnitude. This coincidence means that high viral load is indeed the most important factor setting bags 4 and 7 apart. In the Late-lysis simulation, the *E. huxleyi* bloom collapses much faster after day 17 than in the No-lysis case. In the Early-lysis simulation, *E. huxleyi* biomass is almost constant at $1.5 \mu\text{M-N}$ from day 10 to day 18, which is less than 30% of the maximum concentration in the No-lysis simulation, and then

collapses, whereas from day 15 onward all other living or non-living nitrogen pools are higher than in the No-lysis simulation.

Model DMSP and DMS concentrations

In each new scenario, the simulated DMSP_p , DMSP_d , and DMS concentrations agree better with observations than in the previous one (Fig. 3). Scenario S2 improves the model DMSP_p concentration by increasing the $\text{DMSP}:\text{N}$ ratio under nutrient stress. Scenario S3 avoids DMSP_d accumulation during the first bloom by allowing picophytoplankton to take up DMSP_d . Scenario S4 improves the model DMS concentration during the second bloom by giving a competitive advantage to DMS-consuming bacteria under high DMS concentrations and increasing DMS leakage by *E. huxleyi* cells during viral infections.

The dynamics of DMSP_p (Fig. 3a–d) in the mesocosms are largely correlated with those of chlorophyll. In the observations and in all four scenarios a first maximum occurs on day 9, with around 400 nM, and a second one on day 19, with around 600 nM. In scenario S1, DMSP_p concentration is consistently overestimated by around 50% during the growth phase of the first bloom and underestimated after day 8 during

the inter-bloom. By contrast, scenario S2 reproduces the DMSP_p observations almost perfectly from day 0 to day 11, with a large increase from day 8 to day 9 caused by nutrient stress. Scenarios S3 and S4 share the same DMSP_p concentrations as scenario S2. None of the scenarios correctly reproduces the very low DMSP_p concentration (< 200 nM) on day 13 and the increase in DMSP_p (to > 400 nM) on days 23 and 24, because these two trends of the observations cannot be related to trends in phytoplankton, chlorophyll, or nutrients. In the fjord, all scenarios tend to underestimate DMSP_p content, especially from day 5 to day 12, but scenario S1 more than the others. The discrepancies between model and observations may be caused by changes in phytoplankton composition that DMOS-Bloom cannot precisely resolve.

In contrast to DMSP_p , DMSP_d (Fig. 3e–h) varies significantly between scenarios. In observations from the mesocosms, DMSP_d peaked at 25 nM during the first bloom, and from 50 to 90 nM during the second bloom, depending on the bag. In all four scenarios, the DMSP_d maxima occur at the right time. However, scenarios S1 and S2 experience excessive DMSP_d accumulation during the first bloom, with maxima of 230 nM and 87 nM respectively. This accumulation occurs because bacterial growth follows that of phytoplanktonic

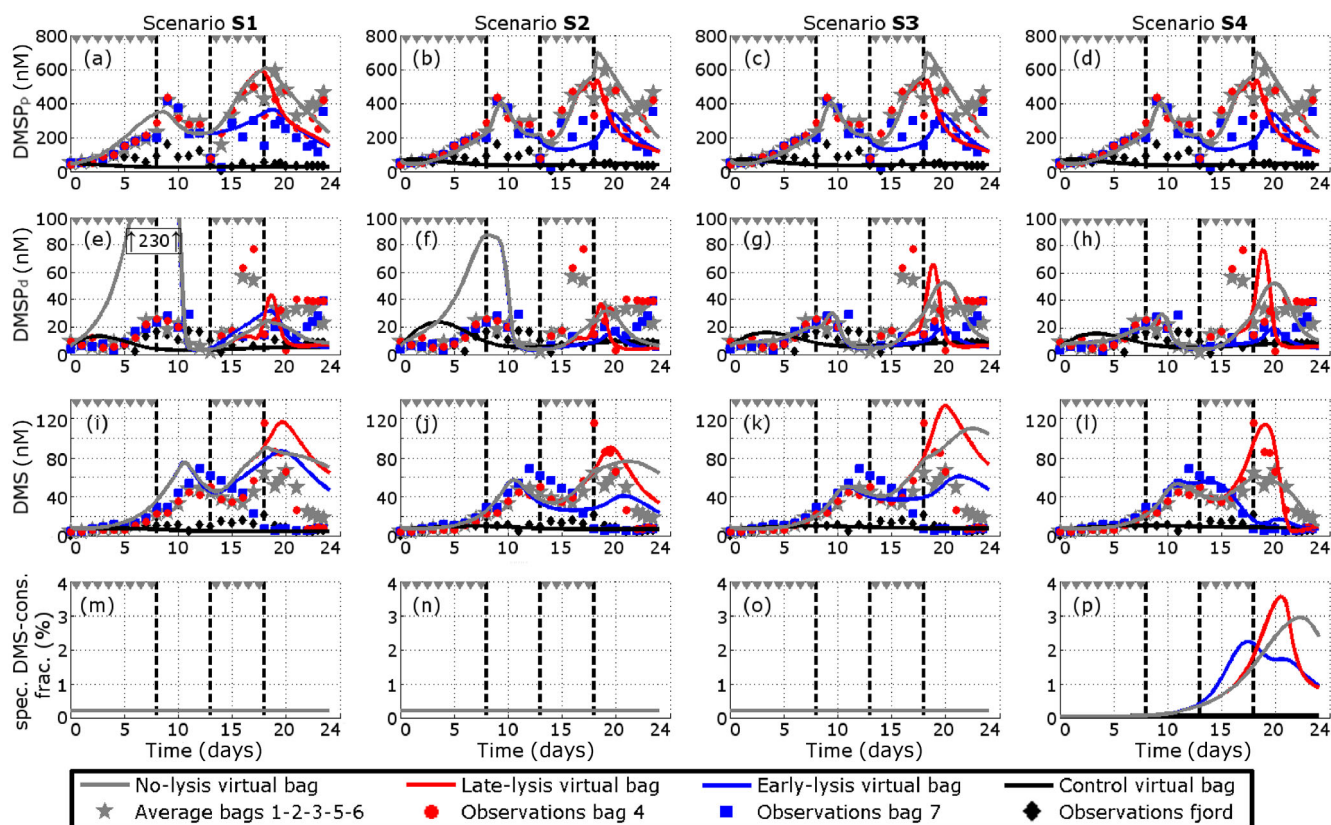


Fig. 3. Model particulate DMSP (upper row), dissolved DMSP (second row) and DMS (third row) concentrations and fraction of specialist DMS-consuming bacteria (lower row) in the four scenarios. Lines and symbols represent model results and observations respectively. Each color represents a virtual bag and the observations it is designed to reproduce.

DMSP producers with a delay of several days, leaving a time window between days 5 and 9 when production is high and consumption by bacteria is low. In scenarios S3 and S4, the correct order of magnitude during both blooms can only be reached by allowing picophytoplankton to take up DMSP_d . We note that during the second bloom, from day 18 on, observations pointed to a relatively constant and high concentration of DMSP_d , between 30 and 40 nM whereas in the model DMSP_d concentration is reduced to less than 20 nM at the end of the experiment. We do not know what mechanism stabilizes DMSP_d concentration at the end of the experiment, when phytoplankton biomass declines and bacterial biomass increases. As DMSP_d production is constrained by DMSP_p content and by mortality rates, the model error is much more likely to be in the DMSP_d turnover rate. It does not affect the overall DMSP_d consumption and the DMS production by bacteria. Errors in the consumption rate can modify the DMSP_d stocks but all the DMSP_d that is produced is consumed anyway.

In all scenarios, DMS concentration (Fig. 3i–l) experiences two peaks, the first of which occurs on day 11, 3 d after the chlorophyll peak, in agreement with observations. However, from scenario S1 to S4, all changes improve the fit of model DMS concentration to observations, for different reasons. Scenarios S1 and S2 overestimate DMS concentration during the first bloom. This mismatch is corrected in scenario S3 by reducing DMSP_p concentration and allowing picophytoplankton to consume DMSP_d , thereby reducing the amount of DMSP_d available for cleavage by bacteria. However, scenarios S1–S3 all fail to represent the rapid DMS decline observed after the second bloom: their DMS concentrations are always larger than 40 nM from day 8 to the end of the experiment. In the virus-infected bags, scenarios S1–S3 also have their DMS maxima later than in the observations.

Scenario S4 is the most accurate of the four scenarios ($R > 0.72$ for DMSP_p and $R > 0.95$ for DMS in the No-lysis, Late-lysis and Early-lysis virtual bags) thanks to two changes. First, DMS production is increased when viral infection is active, allowing DMS concentration to reach its maximum of 120 nM in time in the Late-lysis virtual bag and to remain higher than 50 nM from day 11 to day 15 in the Early-lysis virtual bag (Fig. 3l). Second, the fraction of DMS-consuming bacteria (Fig. 3m–p) is allowed to increase in response to high DMS concentration, going from 0.05% in the fjord and at the beginning of the experiment to 3.0% in the No-lysis virtual bag and even 3.7% in the Late-lysis virtual bag during the demise of the second bloom. With these two changes, the maximum and minimum DMS concentrations from day 18 to day 24 are correctly reproduced in the No-lysis and Late-lysis cases. In bag 7, observed DMS concentration decreases from 50 nM on day 15 to less than 10 nM from day 18 to the end of the experiment, several days earlier than in all other bags. In our model, this trend can only be reproduced by making the growth rate of specialist DMS consumers higher under viral infection, allowing this group to reach 2.3% of the total

bacterial community as early as day 18. Why viral infection accelerates both DMS production and consumption is not yet fully understood.

In the fjord, the model has almost constant DMSP_d and DMS concentrations, whereas the corresponding observations fluctuate around their mean. Scenarios S3 and S4 have a mean fjord DMS concentration 2% smaller than observations and a mean fjord DMSP_d concentration 5% smaller than observations, a very small difference that may stem from the underestimation of DMSP_p or from measurement uncertainties.

DMSP and DMS fluxes

By design, DMOS-Bloom reproduces the concentrations of DMSP_d and DMS by computing their sources and sinks based on established mechanistic equations. One advantage of this modeling approach is that, as long as the model fits observations, it also provides estimates of sources and sinks. Comparison of the fluxes allows us to understand what processes have the largest impact on our state variables and thus how the system would react to environmental changes. In Fig. 4 we display the model fluxes for each virtual bag from the beginning to the end of the experiment, based on scenario S4, which is the most accurate.

In all bags and also in the fjord, the main sources of dissolved DMSP_d (Fig. 4a–d) are grazing and mortality. Therefore, DMSP_d production is aligned in time with phytoplankton death. In all virtual bags, there is a maximum production of 161 nM d^{-1} on day 9, 81% of which is explained by grazing. In the Late-lysis virtual bag, there is a second DMSP_d production maximum of 268 nM d^{-1} around day 18 when the large *E. huxleyi* bloom collapses due to viral infection. During this second peak, mortality accounts for 71% of DMSP_d production. In the fjord, production is never higher than 13 nM d^{-1} and decreases with time as picophytoplankton biomass decreases. Exudation is always a minor source, accounting for 10.7% to 12.9% of DMSP_d production, depending on the bag.

Dissolved DMSP_d has two sinks: consumption by heterotrophic bacteria and consumption by picophytoplankton (Fig. 4e–h). In the fjord, the two sinks have the same order of magnitude, both oscillating between 1.6 and 7.4 nM d^{-1} . In the bags, picophytoplankton is by far the dominant DMSP_d consumer before day 9, and heterotrophic bacteria are the dominant consumers from day 10 on. On average, phytoplankton account for 36% of DMSP_d uptake in the fjord and between 24% and 30% in the bags.

Bacteria are the largest DMS producers overall, by converting dissolved DMSP_d to DMS (Fig. 4i–l). This source accounts for 82% of DMS production in the fjord, 69% in the No-lysis virtual bag, 61% in the Late-lysis case and 71% in the Early-lysis case. However, during the growth phase of *E. huxleyi*, from day 14 to day 18, leakage by phytoplankton cells is the largest DMS source. Leakage is one of the reasons why the DMS maximum occurs at the same time as the chlorophyll maximum during the second bloom. The other reason is the change in the dominant DMS sink.

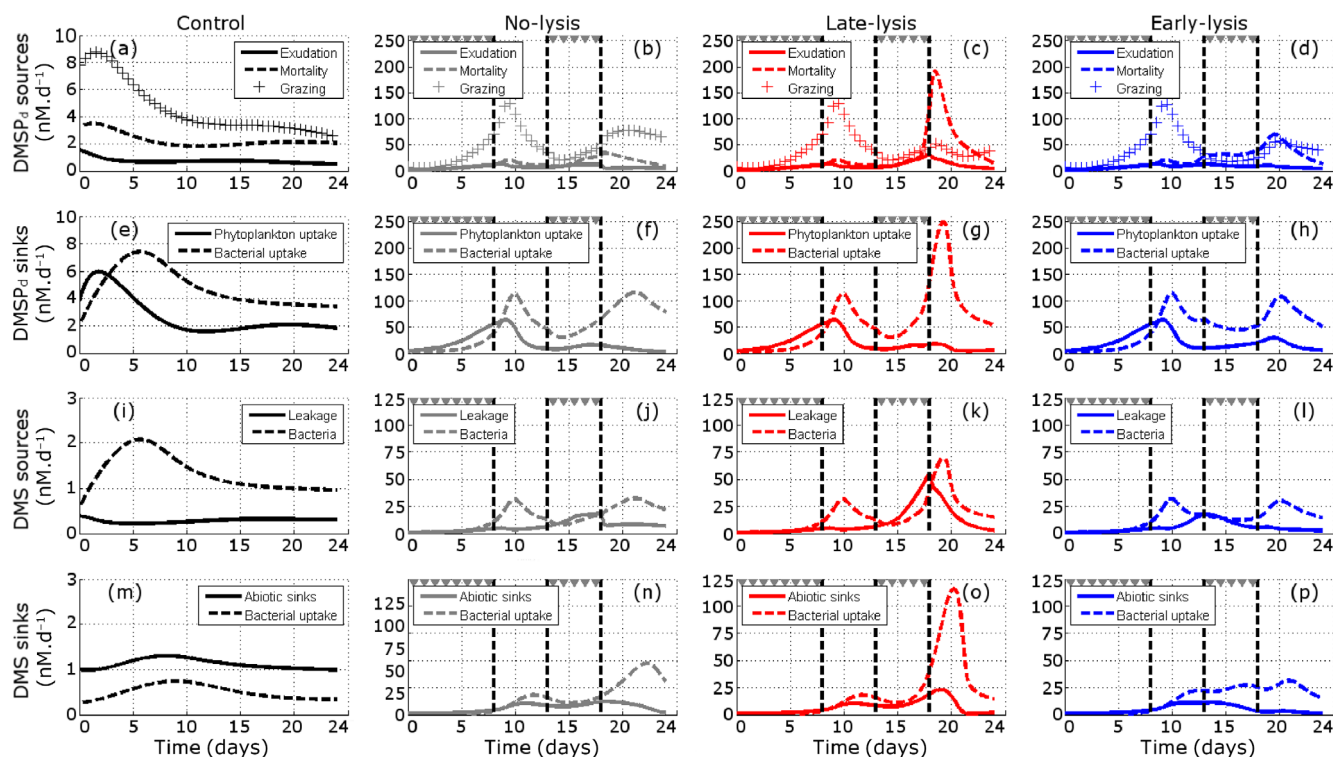


Fig. 4. Model dissolved DMSP and DMS sources and sinks. Note the differences in scale between the Control case (fjord) and the mesocosm bags.

In the fjord, the abiotic DMS sinks account for 69% of DMS losses (Fig. 4m–p). In the mesocosms however, DMS uptake by bacteria is at least 50% of the total DMS losses from day 10 on. During the demise of the second bloom, bacterial DMS uptake is even one order of magnitude larger than the abiotic sinks, explaining why DMS removal is very fast after day 20 in all real and virtual bags.

The average simulated turnover rate constant of $DMSP_d$ (Fig. 5a) in the fjord is 0.8 d^{-1} , which is in the lower range of previous estimates (Galí and Simó 2015; Lizotte et al. 2017). In other words, the residence time of $DMSP_d$ is 1.2 d, with stocks of 9.0 nM and sinks of 7.5 nM d^{-1} . In the bags, the simulated consumption of $DMSP_d$ is faster due to the large populations of consumers. The average residence time is reduced to 0.26 d in the No-lysis virtual bag, 0.19 d in the Late-Lysis case and 0.16 d in the Early-lysis case. During the demise of the first bloom, the turnover rate constants in the mesocosms can temporarily reach more than 13 d^{-1} . In the Late-lysis and Early-lysis virtual bags, our model also diagnoses $DMSP_d$ turnover rate constants larger than 10 d^{-1} during the demise of the second bloom, but these might be overestimates, as DMOS-Bloom underestimates dissolved DMSP stocks at this time in these two virtual bags (Fig. 3h). The same contrast between the fjord and the bags can be seen for the simulated DMS turnover rate constant (Fig. 5b). In the fjord, the DMS turnover rate constant is close to 0.18 d^{-1} , but in the bags during the demise of the second bloom, the DMS

turnover rate constant is larger than 2 d^{-1} . The DMS turnover is faster in bags where a viral infection is ongoing.

As the turnover rate constants vary by one order of magnitude, the DMS and $DMSP_d$ standing stocks are poor predictors of the DMS production and removal. For instance, the DMS production over the whole experiment is 12.8 times larger in the No-lysis virtual bag than in the Control, but the average DMS concentration is only 3.6 times larger in the bag and the DMS residence time there is 3.6 times shorter due to rapid bacterial consumption.

Viral infection increases the DMS yield and DMS production in the Late-lysis virtual bag but not in the Early-lysis one. In the Late-lysis simulation, increased phytoplankton mortality and leakage lead to increased DMS production and yield. In the Early-lysis simulation, DMS production is reduced because *E. huxleyi* biomass is very low, even though high mortality rates enhance specific DMS production. The community DMS yield is also reduced because species that have a lower leakage rate than *E. huxleyi* prevail. Total time-integrated DMS production per unit volume during the second bloom, from day 13 to day 24, is 337 nM in the No-lysis case, 497 nM in the Late-lysis case but 279 nM in the Early-lysis case, with mean DMS yields of 29.6, 39.4, and 26.7% respectively (Fig. 5c).

However, DMS concentration is still a good predictor of emission to the atmosphere, as gas exchange is a physical process independent from biochemical rates. Mean DMS concentration during the second bloom is 43.3 nM in the No-lysis case,

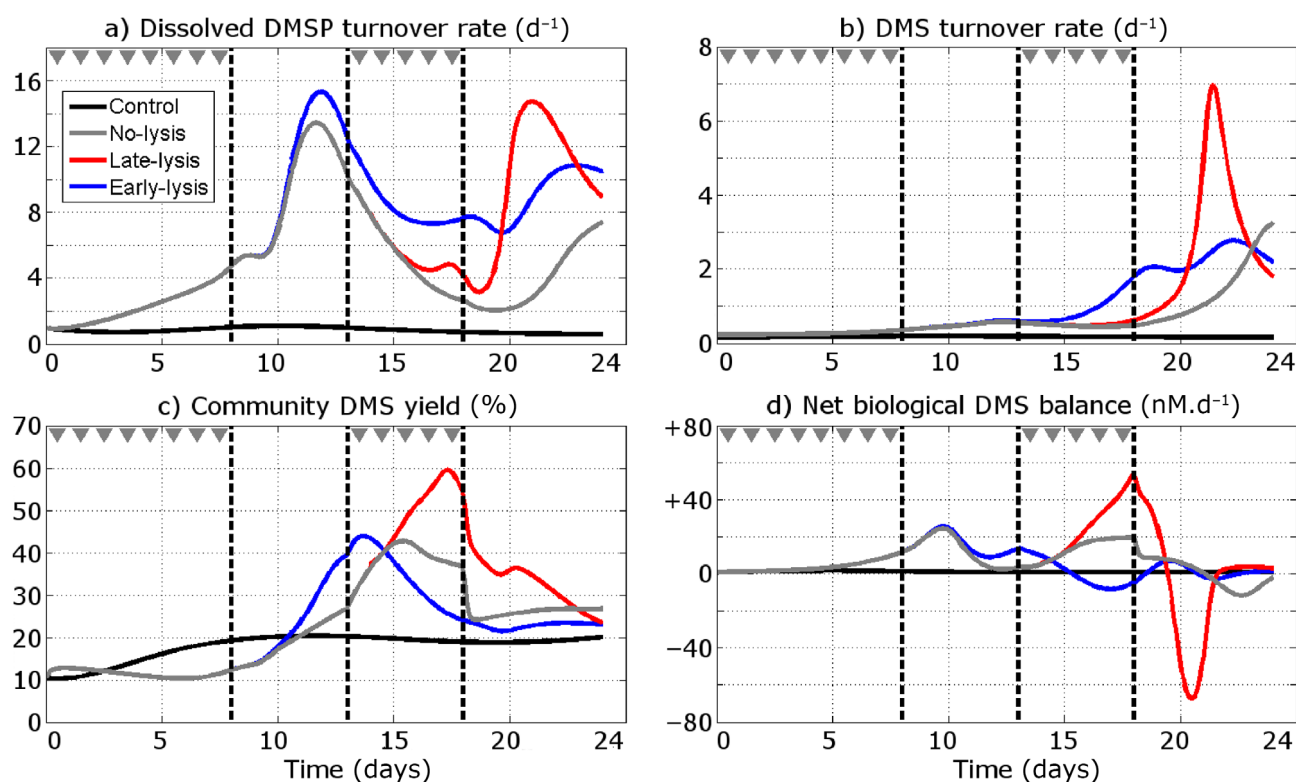


Fig. 5. Model dissolved DMSP and DMS turnover rate constants, community DMS yield and net DMS balance.

49.2 nM in the Late-lysis case, and 25.7 nM in the Early-lysis case. The increase in DMS emission will therefore be modest and within the ensemble standard deviation of bags 1, 2, 3, 5, and 6 ($\pm 28\%$) for viral infections that accelerate bloom demise (Late-lysis), whereas early infections will reduce DMS emission substantially (Early-lysis). Note, however, that temporal emission dynamics differ among cases. High and short lived DMS emission events (spikes) may have different consequences for atmospheric processes than sustained high emissions.

In addition to the above figures, the DMS concentration at the end of the experiment has decreased to its initial value of 10 nM or is on the verge of getting there due to high consumption rates in all the bags. The net biological DMS balance (Fig. 5d) confirms that, by the end of the experiment, a point has been reached where the microbial community has become a net sink of DMS. Any further increase in DMS production, either by nutrient addition or viral lysis, is likely to be rapidly consumed by bacteria and to never reach the atmosphere.

Discussion

Key mechanisms needed to reproduce the organic sulfur cycle

In DMOS-Bloom, DMSP consumption by phytoplankton is necessary to avoid DMSP_d accumulation during the first bloom.

This result is robust because it stems from the temporal patterns of the microbial types. DMSP consumption by picophytoplankton is necessary, not because bacteria cannot consume enough DMSP to account for average observed concentrations, but because bacteria consume DMSP too late. DMSP consumption by phytoplankton has already been observed for cyanobacteria and diatoms, two taxa that produce no or little DMSP, and for picoalgae (Vila-Costa et al. 2006a). By contrast DMSP consumption is thought to be absent or rare in dinoflagellates and haptophytes (Vila-Costa et al. 2006a), which are strong DMSP producers. In our model exercise, we found that a fraction of phytoplankton needed to consume DMSP, at least during the first phytoplankton bloom, when *Micromonas* sp. was the most abundant taxon. Despite being DMSP producers, *Micromonas* has been shown to be attracted by DMSP (Seymour et al. 2010). Alternatively, as the phytoplankton community was diverse during the first bloom, *Micromonas* might not necessarily be the only or even the main phytoplanktonic consumer of DMSP. Cyanobacteria were negligible in the mesocosms, but the nanophytoplanktonic community from the beginning of the experiment to day 9 contained diatom taxa, such as *Rhizosolenia*, *Minutocellus*, *Leptocylindrus*, and *Eucampia* (Vincent et al. 2023). In particular, the *Eucampia* abundance followed a temporal pattern similar to that of *Micromonas*. We cannot exclude that a fraction of nanophytoplankton consumed DMSP during the second

phytoplankton bloom, but this cannot be shown with our mechanistic numerical model.

In our model, the only way to reproduce the rapid decrease in DMS concentration observed after the DMS maximum of day 18 is to allow specialist DMS-consuming bacteria to respond rapidly to the increase in DMS concentration, making the bacterial community a net DMS sink. This DMS collapse cannot be explained by an increase in gas exchange due to the wind: bags 5 and 6 were covered (Vincent et al. 2023) and experienced the same trend in DMS concentration. DMS photolysis by UV radiation did not increase either after day 18. On the contrary, the cloud cover was higher during the demise of the second bloom than during the rest of the experiment (Supplementary Fig. S4). In the Late-lysis virtual bag, a DMS turnover rate constant of 9.3 d^{-1} is estimated for day 22, and more than 97% of that loss is explained by bacteria. DMS loss rates in situ measurements lie between 0.125 and 2 d^{-1} (Galí and Simó 2015), but loss rates larger than 2 d^{-1} have already been reported in artificially induced phytoplankton blooms. For instance, DMS turnover rate constants peaked at 6.5 d^{-1} during the microcosm experiment of Pinhassi et al. (2005), compared to 0.2 d^{-1} in the control experiment. Twelve days after the beginning of an iron fertilization experiment, Merzouk et al. (2006) reported that bacteria acted as a net DMS sink and that DMS concentration collapsed to less than its initial value. Global models would gain from explicitly representing the dynamics of specialist DMS-consuming bacteria, as their growth or decline acts as a damping term on perturbations of the DMS dynamics.

We cannot directly link the observed DMS dynamics to any particular bacterial taxon. However, a likely DMS consumer taxon at the end of the second bloom is *Methylophaga*, obligate methylotrophs able to use DMS as a carbon source (de Zwart et al. 1996; Schäfer 2007) that have been reported to be the most efficient users of DMS carbon in DMS-enriched waters (Vila-Costa et al. 2006b). Indeed, the relative abundance of *Methylophaga* among bacteria, estimated by analyzing the 16S rRNA sequences, increased rapidly from day 15 on (Supplementary Fig. S2) (Vincent et al. 2023) and coincide with the relative abundance of DMS-consuming specialists of our model. We note that, in bag 7, *Methylophaga* relative abundance reached its maximum around day 18, 4 d earlier than in any other bag. *Methylophaga* remained abundant after this maximum, which may explain why DMS concentration was lower than 8 nM in bag 7 from day 18 to the end of the experiment. In DMOS-Bloom, the growth of specialist DMS consumers must be accelerated during viral infections in order to reproduce the above features.

Other known DMS consumers were also observed in the mesocosms, but they are not known to consume DMS as a carbon source and their distribution in time did not coincide with that of DMS consumption. Some were distributed evenly in time (*Glaciecola*), and others had their maximum relative abundance during the first bloom (*Marinobacter*, *Alteromonas*,

Pseudoalteromonas). If these consumers do not bloom in DMS-enriched waters, their DMS consumption will be more stable in time than that of *Methylophaga*, similarly to the DMS consumption by generalist bacteria in DMOS-Bloom.

Potential for improvement and alternative scenarios

The four scenarios presented in our study were built by adding new mechanisms step by step in order to reproduce the main features of the DMSP and DMS observations. Some alternative scenarios have been considered during this study and later abandoned, either because of their complexity, because data to validate them were lacking, or because they failed to improve the fit between model and observations.

During the second bloom, model DMSP_d is less stable in time than observed DMSP_d . In the Late-lysis and Early-lysis virtual bags, large bacterial biomass depresses model DMSP_p concentrations to below 10 nM, whereas observed DMSP_d at the end of all mesocosm experiments are above 20 nM. Li et al. (2015) reported the existence of a DMSP_d pool that is refractory to degradation on a timescale of days. Simulating a refractory DMSP_d pool able to persist throughout the second bloom might increase the fit between model and observations.

Kiene et al. (2000) hypothesized that the bacterial DMS yield depends on DMSP_d concentration and sulfur demand. As DMSP cleavage does not allow bacteria to incorporate its sulfur, it is likely less favored when DMSP concentrations are low and bacterial production is high. In our study, a relatively high bacterial DMS yield of 28% is used to account for high DMS concentrations between the two blooms, when phytoplankton DMS leakage is small. In some way this is in line with the sulfur demand hypothesis, as our mesocosms were very enriched in DMSP_d . However, the time (days 10 to 13) when high bacterial DMS yield is most needed to improve the fit is also the time when the bacterial sulfur demand is highest whereas the dissolved DMSP concentrations are relatively low (around 10 nM). Therefore a variable DMS yield depending on the sulfur demand or sulfur status of bacteria is not useful for our study. This result does not outright invalidate the sulfur demand hypothesis, as other organic compounds produced during a bloom may provide sulfur (Pinhassi et al. 2005).

One organic sulfur compound is lacking in the DMOS-Bloom model: DMSO. DMSO is a product of DMS oxidation by either photolysis or bacteria using widespread non-specific enzymes (Chen et al. 2011). However, the ability to use DMSO as an electron acceptor and to reduce it back to DMS is also widespread among bacteria (Griebler and Slezak 2001) and phytoplankton (Spiese et al. 2009). In our model, we decided not to include DMSO because we lack data to validate its concentration and fluxes. Neglecting a DMS source means we may overestimate other DMS sources or underestimate DMS sinks, particularly the sources and sinks proportional to the bulk bacterial biomass. Indeed, our bacterial DMS yield (28%) is in the upper range of published estimates, whereas our bacterial DMS consumption in the fjord (30% of the total DMS

sink) is in the lower range (Galí and Simó 2015). In past observational studies, bacterial DMS consumption has generally been shown to have the same order of magnitude as photolysis and to be larger than emission to the atmosphere, although variability between measurements is large (Simó and Pedrós-Alió 1999; Bailey et al. 2008; Galí and Simó 2010; Yang et al. 2013). Taking DMSO reduction into account would allow us to use a lower bacterial DMS yield and a higher consumption rate by generalist DMS consumers, without altering the conclusions of our model exercise.

In this study we have neglected the impact of light, UV radiation and water temperature on the organic sulfur cycle. We have assumed that in a shallow environment in summer, light was not limiting for phytoplankton. Indeed, daily-averaged, downwelling photosynthetic active radiation (PAR) at sea surface was stable and always larger than 127 W m^{-2} from day 0 to day 16, which encompasses the first phytoplankton bloom, the inter-bloom, and the onset of the second bloom (Supplementary Fig. S4). Therefore differences in light availability or UV radiation cannot explain the trends observed during this period of time. During the demise of the second bloom, from day 18 onward, there have been several days with large cloud cover and low surface solar irradiance, but on average during this period the PAR was still 72 W m^{-2} at surface and 33 W m^{-2} integrated over the water column of the mesocosms, which is likely not limiting or less limiting than nutrients for most phytoplankton species (Edwards et al. 2015). If DMS photolysis were slower during the demise of the second bloom than during the previous phases due to lower UV radiation, then our conclusion that DMS consumption by bacteria at that time is very fast would be even stronger. Water temperature varies by less than 0.4° between bags but is on average 3° warmer from day 8 to day 18 than earlier or later in the experiment (Supplementary Fig. S5). To our knowledge, small short-term temperature changes in natural microbial communities have never been shown to change the dynamics of DMSP and DMS concentrations.

Bacterial DMS consumption and implications for deliberate fertilization experiments

In our mesocosm experiments, nutrient enrichment led to a temporary increase in DMS concentration. Indeed, during the 24 d of the experiment, the DMS concentration was on average 220% larger in the mesocosms than in the fjord, and therefore DMS emission to the atmosphere increased in proportion. This was a transient process: by the end of the experiment DMS concentration had collapsed to its initial values. Similar transient DMS increases have also been observed in previous mesocosm experiments performed in Raunefjorden (Vogt et al. 2008a; Avgoustidi et al. 2012).

However, past studies also showed that in other natural environments, deliberate induced fertilization has a smaller impact on DMS emission, if it has an impact at all. For instance, in an open ocean iron fertilization experiment in the

Northeast Pacific, Levasseur et al. (2006) measured an increase in DMS concentration during the first 2 weeks of the experiment and then a decrease to concentrations lower than the control unfertilized patch. Belviso et al. (2008) observed that the phytoplankton blooms caused by natural iron enrichment over the Kerguelen Plateau did not translate into higher DMS production. Back-of-the-envelope estimates of deliberate iron fertilization in the Southern Ocean also suggest little impact on DMS emission to the atmosphere (Vogt et al. 2008b). Several reasons might explain the contrast between these open ocean iron enrichment experiments and our nitrogen-limited mesocosm experiments. The iron-induced blooms were dominated by diatoms, which generally produce less DMSP than *E. huxleyi* (Stefels et al. 2007) and lack DMSP-lyase entirely. Iron addition may also have decreased the phytoplankton DMSP:C ratio more than nitrate addition (Sunda et al. 2002).

Comparisons between our study and previous enrichment experiments tell us that deliberate fertilization can increase DMS emission to the atmosphere provided (1) the bloom is dominated by DMSP producers, and (2) fertilization does not extend more than a few weeks in time, as DMS consumers set an absolute limit to the DMS emissions, even when the phytoplankton bloom is dominated by DMS producers. Increased nutrient availability can only increase DMS concentration, and therefore DMS emission, during a transient regime.

Does viral infection affect DMS production?

Grazing and viral lysis are the main causes of phytoplankton death in our model. Both contribute to DMS production by releasing DMSP_d into the environment where bacteria can convert it to DMS. When a phytoplankton cell is lysed by a virus, all its particulate DMSP is released into seawater as dissolved DMSP (Hill et al. 1998). When a phytoplankton cell is grazed, an estimated 30–45% of phytoplankton DMSP is retained or assimilated into proteins by the predator (Simó et al. 2002; Saló et al. 2009). Therefore, a given phytoplankton cell will release 30–45% less DMSP and induce less bacterial DMS production if it is grazed than if it is lysed. However, assessing what cause of cell death produces more DMS is not as straightforward for phytoplankton that contain DMSP-lyase. By mixing DMSP and DMSP-lyase, both grazing and viral mortality can convert a fraction of phytoplankton DMSP to DMS, and one process may have a larger yield than the other. For instance, Evans et al. (2007) showed that viral infection reduces the activity of DMSP-lyase in *E. huxleyi*. As a consequence, in axenic conditions, viral infection of a single strain of *E. huxleyi* produced less DMS per consumed cell than grazing by the dinoflagellate *Oxyrrhis marina*. Phytoplankton intra-specific diversity makes prediction even more difficult. DMS and acrylate have antiviral properties which make the *E. huxleyi* strains with large DMSP-lyase activity more resistant to infection (Evans et al. 2006). During infection of a population with several strains with different DMSP-lyase activities, the proportion of resistant cells may increase due to the

death of their competitors, which may in turn increase DMS production.

In addition, viral infections also modify in two opposite ways the number of cells that die and release DMSP. Infection releases nutrients to the environment, which may accelerate phytoplankton growth. If the phytoplankton population remains high enough, its life cycle will be accelerated, and more organic matter, including DMS, will be released. However, a strong infection may depress the overall amount of phytoplankton to the point where, even with more nutrients, the total production of organic matter is reduced. Which effect is stronger depends on the context.

In our study, viral mortality differed between bags, allowing us to estimate the overall effect of viruses on DMS production in two contrasting cases, regardless of the biochemical mechanisms at stake. In bag 7, where viral lysis became a large mortality term at an early stage, *E. huxleyi* remained stable at moderate biomass, and the chlorophyll concentration was lower than in other bags as other phytoplankton species benefited little from the demise of *E. huxleyi*. The community DMS yield and DMS production were lower than in the other bags. In this early lysis case, the largest effect of viruses was to depress the concentration of their host and of every chemical their host produces. In bag 4, viral lysis decimated *E. huxleyi* at a later stage, when the chlorophyll maximum had already been reached, and only accelerated the bloom demise. In this late lysis case, the maximum DMS concentration was 75% higher than in the average of bags 1, 2, 3, 5, and 6, in spite of the larger biomass of DMS-consuming bacteria. In the model, total DMS production during the second bloom has to be 50% higher in the Late-lysis virtual bag than in the No-Lysis case and the maximum DMS yield 40% higher in order to account for the observations. This contrast highlights the bloom stage dependence of viral infection on DMS production in natural ecosystems.

Conclusions

The DMOS-Bloom model is used to test hypotheses on key processes involving DMSP and DMS. We show that particulate DMSP can only be correctly reproduced if DMSP concentration per cell increases under nutrient stress. A fraction of phytoplankton must also be allowed to consume dissolved DMSP in order to avoid DMSP_d accumulation at concentrations larger than 80 nM during the first bloom: heterotrophic bacteria cannot be the only DMSP_d consumers. The observed collapse in DMS concentrations during the demise of the second bloom cannot be explained unless the fraction of specialist DMS-consuming bacteria increases over the experiment in a delayed response to high DMS concentrations. On a timescale of 2–3 weeks, nutrient enrichment can greatly increase DMS emission to the atmosphere provided that the induced phytoplankton bloom is dominated by DMSP producers. Adding nutrients on longer timescales is unlikely to increase DMS emission further because the overwhelming majority of the

DMS produced after 3 weeks would be rapidly consumed by bacteria and thus would never reach the atmosphere.

The trends observed during the second bloom in the virus-infected bags imply that infection increases DMS production per unit of chlorophyll but also decreases the abundance of phytoplankton and accelerates the growth of specialist DMS consumers. The overall impact of viruses on DMS emission depends on the balance between these three effects. If viral infection occurs early and prevents the *E. huxleyi* bloom, the overall effect is a damping of total DMS production and emission. If viral infection occurs late and only accelerates the bloom demise, total DMS production is increased, which may translate into higher DMS emission during a transient regime. This transient regime cannot be sustained for more than a few days because DMS consumers respond by increasing their abundance even faster than during uninfected blooms.

Data availability statement

The code and data of DMOS-Bloom are freely available on GitHub (<https://github.com/Guillaume%20LeGland/DMOS-Bloom>) and Zenodo (<https://doi.org/10.5281/zenodo.7944840>) under the MIT license. The DMOS-Bloom code was designed to run on open-source GNU-Octave (tested on version 4.4.1) and on MATLAB (tested on version R2010b). The execution has been tested on Windows with a 2.5-GHz Intel i5-3210M processor, on Linux Ubuntu with a 2.4-GHz Intel Xeon E5645 processor, and on Linux Debian with a 2.6-GHz Intel Xeon E5-2640 processor. The main code modules are:

- DMOS_Bloom is the main script to launch DMOS-Bloom, calling all functions.
- DMOS_Bloom_keys is the function where the different options are declared.
- DMOS_Bloom_parameters is the function where the values of the model parameters are assigned.
- DMOS_Bloom_ode45eqs is a function called at each time step to solve the ordinary differential equations of the DMOS-BLOOM model.

DMOS-Bloom also contains other functions to load data, plot figures, and optimize model parameters. The DATA folder contains two input files: BERGEN-DATA.csv and BERGEN-DMS-CONSUMERS.csv. BERGEN-DATA.csv contains observations of phytoplankton and heterotrophic bacteria abundances and of nitrate, particulate DMSP, dissolved DMSP and DMS concentrations. BERGEN-DMS-CONSUMERS.csv contains the relative abundances of the DMS-consuming taxa measured during the experiment. Once all files are loaded, DMOS-Bloom is launched simply by calling the DMOS-Bloom script.

References

- Alcolombri, U., S. Ben-Dor, E. Feldmesser, Y. Levin, D. S. Tawfik, and A. Vardi. 2015. Identification of the algal dimethylsulfide-releasing enzyme: A missing link in the

- marine sulfur cycle. *Science* **348**: 1466–1469. doi:[10.1126/science.aab1586](https://doi.org/10.1126/science.aab1586)
- Archer, S. D., M. Ragni, R. Webster, R. L. Airs, and R. J. Geider. 2010. Dimethyl sulfoniopropionate and dimethyl sulfide production in response to photoinhibition in *Emiliania huxleyi*. *Limnol. Oceanogr.* **55**: 1579–1589. doi:[10.4319/lo.2010.55.4.1579](https://doi.org/10.4319/lo.2010.55.4.1579)
- Asher, E. C., J. W. H. Dacey, M. M. Mills, K. R. Arrigo, and P. D. Tortell. 2011. High concentrations and turnover rates of DMS, DMSP and DMSO in Antarctic Sea ice. *Geophys. Res. Lett.* **38**: 609. doi:[10.1029/2011GL049712](https://doi.org/10.1029/2011GL049712)
- Avgoustidi, V., P. D. Nightingale, I. Joint, M. Steinke, S. M. Turner, F. E. Hopkins, and P. S. Liss. 2012. Decreased marine dimethyl sulfide production under elevated CO₂ levels in mesocosm and in vitro studies. *Environ. Chem.* **9**: 399. doi:[10.1071/en11125](https://doi.org/10.1071/en11125)
- Bailey, K. E., and others. 2008. Dimethylsulfide production in Sargasso Sea eddies. *Deep Sea Res. II Topic. Stud. Oceanogr.* **55**: 1491–1504. doi:[10.1016/j.dsr2.2008.02.011](https://doi.org/10.1016/j.dsr2.2008.02.011)
- Belviso, S., and others. 2008. Effect of natural iron fertilization on the distribution of DMS and DMSP in the Indian sector of the Southern Ocean. *Deep Sea Res. II Topic. Stud. Oceanogr.* **55**: 893–900. doi:[10.1016/j.dsr2.2007.12.040](https://doi.org/10.1016/j.dsr2.2007.12.040)
- Benner, R., and R. M. W. Amon. 2015. The size-reactivity continuum of major bioelements in the ocean. *Annu. Rev. Mar. Sci.* **7**: 185–205. doi:[10.1146/annurev-marine-010213-135126](https://doi.org/10.1146/annurev-marine-010213-135126)
- Bock, J., and others. 2021. Evaluation of ocean dimethylsulfide concentration and emission in CMIP6 models. *Biogeosciences* **18**: 3823–3860. doi:[10.5194/bg-18-3823-2021](https://doi.org/10.5194/bg-18-3823-2021)
- Breckels, M. N., E. C. Roberts, S. D. Archer, G. Malin, and M. Steinke. 2011. The role of dissolved infochemicals in mediating predator-prey interactions in the heterotrophic dinoflagellate *Oxyrrhis marina*. *J. Plankton Res.* **33**: 629–639. doi:[10.1093/plankt/fbq114](https://doi.org/10.1093/plankt/fbq114)
- Brévière, E. H. G., and others. 2015. Surface ocean-lower atmosphere study: Scientific synthesis and contribution to Earth system science. *Antropocene* **12**: 54–68. doi:[10.1016/j.ancene.2015.11.001](https://doi.org/10.1016/j.ancene.2015.11.001)
- Bucciarelli, E., and W. G. Sunda. 2003. Influence of CO₂, nitrate, phosphate, and silicate limitation on intracellular dimethylsulfoniopropionate in batch cultures of the coastal diatom *Thalassiosira pseudonana*. *Limnol. Oceanogr.* **48**: 2256–2265. doi:[10.2307/3597827](https://doi.org/10.2307/3597827)
- Charlson, R., J. E. Lovelock, M. O. Andreae, and S. G. Warren. 1987. Oceanic phytoplankton, atmospheric sulphur, cloud albedo and climate. *Nature* **326**: 655–661. doi:[10.1038/326655a0](https://doi.org/10.1038/326655a0)
- Chen, Y., N. A. Patel, A. Crombie, J. H. Scrivens, and J. C. Murrell. 2011. Bacterial flavin-containing monooxygenase is trimethylamine monooxygenase. *Proc. Natl. Acad. Sci. USA* **108**: 17791–17796. doi:[10.1073/pnas.1112928108](https://doi.org/10.1073/pnas.1112928108)
- de Zwart, J. M. M., P. N. Nelisse, and J. G. Kuenen. 1996. Isolation and characterization of *Methylophaga sulfidovorans* sp. nov.: An obligately methylotrophic, aerobic, dimethylsulfide oxidizing bacterium from a microbial mat. *FEMS Microb. Ecol.* **20**: 261–270. doi:[10.1111/j.1574-6941.1996.tb00324.x](https://doi.org/10.1111/j.1574-6941.1996.tb00324.x)
- Edwards, K. F., M. K. Thomas, C. A. Klausmeier, and E. Litchman. 2015. Light and growth in marine phytoplankton: Allometric, taxonomic, and environmental variation. *Limnol. Oceanogr.* **60**: 540–552. doi:[10.1002/lno.10033](https://doi.org/10.1002/lno.10033)
- Evans, C., G. Malin, W. H. Wilson, and P. S. Liss. 2006. Infectious titres of *Emiliania huxleyi* virus 86 are reduced by exposure to millimolar dimethyl sulfide and acrylic acid. *Limnol. Oceanogr.* **51**: 2468–2471. doi:[10.4319/lo.2006.51.5.2468](https://doi.org/10.4319/lo.2006.51.5.2468)
- Evans, C., S. V. Kadner, L. J. Darroch, W. H. Wilson, P. S. Liss, and G. Malin. 2007. The relative significance of viral lysis and microzooplankton grazing as pathways of dimethylsulfoniopropionate (DMSP) cleavage: An *Emiliania huxleyi* culture study. *Limnol. Oceanogr.* **52**: 1036–1045. doi:[10.4319/lo.2007.52.3.1036](https://doi.org/10.4319/lo.2007.52.3.1036)
- Galí, M., and R. Simó. 2010. Occurrence and cycling of dimethylated sulfur compounds in the Arctic during summer receding of the ice edge. *Mar. Chem.* **122**: 105–117. doi:[10.1016/j.marchem.2010.07.003](https://doi.org/10.1016/j.marchem.2010.07.003)
- Galí, M., E. Devred, M. Levasseur, S.-J. Royer, and M. Babin. 2015. A remote sensing algorithm for planktonic dimethylsulfoniopropionate (DMSP) and an analysis of global patterns. *Remote Sens. Environ.* **171**: 171–184. doi:[10.1016/j.rse.2015.10.012](https://doi.org/10.1016/j.rse.2015.10.012)
- Galí, M., and R. Simó. 2015. A meta-analysis of oceanic DMS and DMSP cycling processes: Disentangling the summer paradox. *Global Biogeochem. Cycles* **29**: 496–515. doi:[10.1002/2014GB004940](https://doi.org/10.1002/2014GB004940)
- Galí, M., and others. 2016. CDOM sources and photobleaching control quantum yields for oceanic DMS photolysis. *Environ. Sci. Tech.* **50**: 13361–13370. doi:[10.1021/acs.est.6b04278](https://doi.org/10.1021/acs.est.6b04278)
- Green, D. H., D. M. Shenoy, M. C. Hart, and A. D. Hatton. 2011. Coupling of dimethylsulfide oxidation to biomass production by a marine flavobacterium. *Appl. Environ. Microbiol.* **77**: 3137–3140. doi:[10.1128/aem.02675-10](https://doi.org/10.1128/aem.02675-10)
- Griebler, C., and D. Slezak. 2001. Microbial activity in aquatic environments measured by dimethyl sulfoxide reduction and intercomparison with commonly used methods. *Appl. Environ. Microbiol.* **67**: 100–109. doi:[10.1128/AEM.67.1.100-109.2001](https://doi.org/10.1128/AEM.67.1.100-109.2001)
- Harada, H., M. Vila-Costa, J. Cebrian, and R. P. Kiene. 2009. Effects of UV radiation and nitrate limitation on the production of biogenic sulfur compounds by marine phytoplankton. *Aquat. Bot.* **90**: 37–42. doi:[10.1016/j.aquabot.2008.05.004](https://doi.org/10.1016/j.aquabot.2008.05.004)
- Hatton, A. D., D. M. Shenoy, M. C. Hart, A. Mogg, and D. H. Green. 2012. Metabolism of DMSP, DMS and DMSO by the cultivable bacterial community associated with the DMSP-producing dinoflagellate *Scrippsiella trochoidea*. *Biogeochemistry* **110**: 131–146. doi:[10.1007/s10533-012-9702-7](https://doi.org/10.1007/s10533-012-9702-7)

- Hill, R. W., B. A. White, M. T. Cottrell, and J. W. H. Dacey. 1998. Virus-mediated total release of dimethylsulfoniopropionate from marine phytoplankton: A potential climate process. *Aquat. Microb. Ecol.* **14**: 1–6. doi:10.3354/AME014001
- Hulswar, S., R. Simó, T. G. Bell, A. Lana, S. Inamdar, P. R. Halloran, G. Manville, and A. S. Mahajan. 2022. Third revision of the global surface dimethyl sulfide climatology (DMS-Rev3). *Earth Syst. Sci. Data* **14**: 2963–2987. doi:10.5194/essd-14-2963-2022
- Keller, M. D. 1989. Dimethyl sulfide production and marine phytoplankton: The importance of species composition and cell size. *Biol. Oceanogr.* **6**: 375–382. doi:10.1080/01965581.1988.10749540
- Kettle, A. J., and M. O. Andreae. 2000. Flux of dimethylsulfide from the oceans: A comparison of updated data sets and flux models. *J. Geophys. Res. Atmos.* **105**: 26793–26808. doi:10.1029/2000JD900252
- Kiene, R. P., L. J. Linn, J. González, M. A. Moran, and J. A. Bruton. 1999. Dimethylsul foniopropionate and methanethiol are important precursors of methionine and protein-sulfur in marine bacterioplankton. *Appl. Environ. Microbiol.* **65**: 4549–4558. doi:10.1128/aem.65.10.4549-4558.1999
- Kiene, R. P., and L. J. Linn. 2000a. The fate of dissolved dimethylsulfoniopropionate (DMSP) in seawater: Tracer studies using ³⁵S-DMSP. *Geochim. Cosmochim. Acta* **64**: 2797–2810. doi:10.1016/S0016-7037(00)00399-9
- Kiene, R. P., and L. J. Linn. 2000b. Distribution and turnover of dissolved DMSP and its relationship with bacterial production and dimethylsulfide in the Gulf of Mexico. *Limnol. Oceanogr.* **45**: 846–861. doi:10.4319/lo.2000.45.4.0849
- Kiene, R. P., L. J. Linn, and J. A. Bruton. 2000. New and important roles for DMSP in marine microbial communities. *J. Sea Res.* **43**: 209–224. doi:10.1016/S1385-1101(00)00023-X
- Kloster, S., J. Feichter, E. Maier-Reimer, K. D. Six, P. Stier, and P. Wetzell. 2006. DMS cycle in the marine ocean-atmosphere system—A global model study. *Biogeosciences* **3**: 29–51. doi:10.5194/bgd-2-1067-2005
- Kuhlisch, C., G. Schleyer, N. Shahaf, F. Vincent, D. Schatz, and A. Vardi. 2021. Viral infection of algal blooms leaves a unique metabolic footprint on the dissolved organic matter in the ocean. *Sci. Adv.* **7**: eabf4680. doi:10.1126/sciadv.abf4680
- Kulmala, M., T. Petäjä, M. Ehn, J. Thornton, M. Sipilä, D. R. Worsnop, and V.-M. Kerminen. 2014. Chemistry of atmospheric nucleation: On the recent advances on precursor characterization and atmospheric cluster composition in connection with atmospheric new particle formation. *Annu. Rev. Phys. Chem.* **65**: 21–37. doi:10.1146/annurev-physchem-040412-110014
- Lana, A., and others. 2011. An updated climatology of surface dimethylsulfide concentrations and emission fluxes in the global ocean. *Global Biogeochem. Cycl.* **25**: GB1004. doi:10.1029/2010GB003850
- Levasseur, M., and others. 2006. DMSP and DMS dynamics during a mesoscale iron fertilization experiment in the Northeast Pacific—Part I: Temporal and vertical distributions. *Deep Sea Res. II Topic. Stud. Oceanogr.* **53**: 2353–2369. doi:10.1016/j.dsr2.2006.05.023
- Li, C., G.-P. Yang, D. J. Kieber, J. Motard-Côté, and R. P. Kiene. 2015. Assessment of DMSP turnover reveals a non-bioavailable pool of dissolved DMSP in coastal waters of the Gulf of Mexico. *Environ. Chem.* **13**: 266–279. doi:10.1071/EN15052
- Lizotte, M., M. Levasseur, C. S. Law, C. F. Walker, K. A. Safi, A. Marriner, and R. P. Kiene. 2017. Dimethylsulfoniopropionate (DMSP) and dimethyl sulfide (DMS) cycling across contrasting biological hotspots of the New Zealand subtropical front. *Ocean Sci.* **13**: 961–982. doi:10.5194/os-13-961-2017
- Marañón, E., P. Cermeño, D. C. López-Sandoval, T. Rodríguez-Ramos, C. Sobrino, M. Huete-Ortega, J. M. Blanco, and J. Rodríguez. 2013. Unimodal size scaling of phytoplankton growth and the size dependence of nutrient uptake and use. *Ecol. Lett.* **16**: 371–379. doi:10.1111/ele.12052
- McParland, E. L., and N. M. Levine. 2019. The role of differential DMSP production and community composition in predicting variability of global surface DMSP concentrations. *Limnol. Oceanogr.* **64**: 757–773. doi:10.1002/lno.11076
- Merzouk, A., M. Levasseur, M. G. Scarratt, S. Michaud, R. B. Rivkin, M. S. Hale, R. P. Kiene, N. M. Price, and W. K. W. Li. 2006. Dmsp and dms dynamics during a mesoscale iron fertilization experiment in the Northeast Pacific—Part II: Biological cycling. *Deep Sea Res. II Topic. Stud. Oceanogr.* **53**: 2370–2383. doi:10.1016/j.dsr2.2006.05.022
- Miller, T. R., K. Hnilicka, A. Dziedzic, P. Desplats, and R. Belas. 2004. Chemotaxis of *Silicibacter* sp. strain TM1040 toward dinoflagellate products. *Appl. Environ. Microbiol.* **2004**: 4692–4701. doi:10.1128/AEM.70.8.4692-4701.2004
- Moran, M. A., C. R. Reisch, R. P. Kiene, and W. B. Whitman. 2012. Genomic insights into bacterial DMSP transformations. *Annu. Rev. Mar. Sci.* **4**: 523–542. doi:10.1146/annurev-marine-120710-100827
- Pinhassi, J., R. Simó, J. M. González, M. Vila, L. Alonso-Sáez, R. P. Kiene, M. A. Moran, and C. Pedrós-Alió. 2005. Dimethylsulfoniopropionate turnover is linked to the composition and dynamics of the bacterioplankton assemblage during a microcosm phytoplankton bloom. *Appl. Environ. Microbiol.* **71**: 7650–7660. doi:10.1128/AEM.71.12.7650-7660.2005
- Quinn, P. K., and T. S. Bates. 2011. The case against climate regulation via oceanic phytoplankton sulphur emissions. *Nature* **480**: 51–56. doi:10.1038/nature10580
- Saló, V., R. Simó, M. Vila-Costa, and A. Calbet. 2009. Sulfur assimilation by *Oxyrrhis marina* feeding on a ³⁵S-DMSP-labelled prey. *Environ. Microbiol.* **11**: 3063–3072. doi:10.1111/j.1462-2920.2009.02011.x
- Schäfer, H. 2007. Isolation of *Methylophaga* spp. from marine dimethylsulfide-degrading enrichment cultures and

- identification of polypeptides induced during growth on dimethylsulfide. *Appl. Environ. Microbiol.* **73**: 2580–2591. doi:[10.1128/aem.02074-06](https://doi.org/10.1128/aem.02074-06)
- Seymour, J. R., R. Simó, T. Ahmed, and R. Stocker. 2010. Chemoattraction to dimethylsulfonio propionate throughout the marine microbial food web. *Science* **329**: 342–345.
- Simó, R. 2004. From cells to globe: Approaching the dynamics of DMS(P) in the ocean at multiple scales. *Can. J. Fish. Aquat. Sci.* **61**: 673–684. doi:[10.1139/f04-030](https://doi.org/10.1139/f04-030)
- Simó, R., and C. Pedrós-Alió. 1999. Role of vertical mixing in controlling the oceanic production of dimethyl sulphide. *Nature* **402**: 396–399. doi:[10.1038/46516](https://doi.org/10.1038/46516)
- Simó, R., S. D. Archer, C. Pedrós-Alió, L. Gilpin, and C. E. Stelfox-Widdicombe. 2002. Coupled dynamics of dimethylsulfoniopropionate and dimethylsulfide cycling and the microbial food web in surface waters of the North Atlantic. *Limnol. Oceanogr.* **47**: 53–61. doi:[10.4319/lo.2002.47.1.0053](https://doi.org/10.4319/lo.2002.47.1.0053)
- Simó, R., M. Vila-Costa, L. Alonso-Sáez, C. Cardelús, Ó. Guadayol, E. Vázquez-Domínguez, and J. M. Gasol. 2009. Annual DMSP contribution to S and C fluxes through phytoplankton and bacterioplankton in a NW mediterranean coastal site. *Aquat. Microb. Ecol.* **57**: 43–55. doi:[10.3354/ame01325](https://doi.org/10.3354/ame01325)
- Spielmeier, A., B. Gebser, and G. Pohnert. 2011. Investigations of the uptake of dimethylsulfonio propionate by phytoplankton. *Chembiochem* **12**: 2276–2279. doi:[10.1002/cbic.201100416](https://doi.org/10.1002/cbic.201100416)
- Spiese, C. E., D. J. Kieber, and C. T. Nomura. 2009. Reduction of dimethylsulfoxide to dimethylsulfide by marine phytoplankton. *Limnol. Oceanogr.* **54**: 560–570. doi:[10.4319/lo.2009.54.2.0560](https://doi.org/10.4319/lo.2009.54.2.0560)
- Stefels, J. 2000. Physiological aspects of the production and conversion of dmsp in marine algae and higher plants. *J. Sea Res.* **43**: 183–197. doi:[10.1016/S1385-1101\(00\)00030-7](https://doi.org/10.1016/S1385-1101(00)00030-7)
- Stefels, J., M. Steinke, S. Turner, G. Malin, and S. Belviso. 2007. Environmental constraints on the production and removal of the climatically active gas dimethylsulphide (DMS) and implications for ecosystem modelling. *Biogeochemistry* **83**: 245–275. doi:[10.1007/s10533-007-9091-5](https://doi.org/10.1007/s10533-007-9091-5)
- Strom, S., G. Wolfe, A. Slajer, S. Lambert, and J. Clough. 2003. Chemical defense in the microplankton II: Inhibition of protist feeding by β -dimethylsulfoniopropionate (DMSP). *Limnol. Oceanogr.* **48**: 230–237. doi:[10.4319/lo.2003.48.1.0230](https://doi.org/10.4319/lo.2003.48.1.0230)
- Sunda, W., D. J. Kieber, R. P. Kiene, and S. Huntsman. 2002. An antioxidant function for DMSP and DMS in marine algae. *Nature* **418**: 317–320. doi:[10.1038/nature00851](https://doi.org/10.1038/nature00851)
- Toole, D. A., D. J. Kieber, R. P. Kiene, D. A. Siegel, and N. B. Nelson. 2003. Photolysis and the dimethylsulfide (DMS) and summer paradox in the Sargasso Sea. *Limnol. Oceanogr.* **48**: 1088–1100. doi:[10.4319/lo.2003.48.3.1088](https://doi.org/10.4319/lo.2003.48.3.1088)
- Tripp, H. J., J. B. Kitner, M. S. Schwalbach, J. W. H. Dacey, L. J. Wilhelm, and S. J. Giovannoni. 2008. SAR11 marine bacteria require exogenous reduced sulphur for growth. *Nature* **452**: 741–744. doi:[10.1038/nature06776](https://doi.org/10.1038/nature06776)
- Twomey, S. 1974. Pollution and the planetary albedo. *Atmos. Environ.* **8**: 1251–1256. doi:[10.1016/0004-6981\(74\)90004-3](https://doi.org/10.1016/0004-6981(74)90004-3)
- Vairavamurthy, A., M. Andreae, and R. Iverson. 1985. Biosynthesis of dimethylsulfide and dimethyl propiothetin by *Hymenomonas carterae* in relation to sulfur source and salinity variations. *Limnol. Oceanogr.* **30**: 59–70. doi:[10.4319/lo.1985.30.1.0059](https://doi.org/10.4319/lo.1985.30.1.0059)
- Vallina, S. M., R. Simó, T. R. Anderson, A. Gabric, R. Cropp, and J. M. Pacheco. 2008. A dynamic model of oceanic sulfur (DMOS) applied to the Sargasso Sea: Simulating the dimethyl sulfide (DMS) summer paradox. *J. Geophys. Res. Biogeosci.* **113**: G01009. doi:[10.1029/2007JG000415](https://doi.org/10.1029/2007JG000415)
- Veres, P. R., and others. 2020. Global airborne sampling reveals a previously unobserved dimethyl sulfide oxidation mechanism in the marine atmosphere. *Proc. Natl. Acad. Sci. USA* **117**: 4505–4509. doi:[10.1073/pnas.1919344117](https://doi.org/10.1073/pnas.1919344117)
- Vila-Costa, M., R. Simó, H. Harada, J. M. Gasol, D. Slezak, and R. P. Kiene. 2006a. Dimethylsulfoniopropionate uptake by marine phytoplankton. *Science* **314**: 652–654. doi:[10.1126/science.1131043](https://doi.org/10.1126/science.1131043)
- Vila-Costa, M., D. A. del Valle, J. M. González, D. Slezak, R. P. Kiene, O. Sánchez, and R. Simó. 2006b. Phylogenetic identification and metabolism of marine dimethylsulfide-consuming bacteria. *Environ. Microbiol.* **8**: 2189–2200. doi:[10.1111/j.1462-2920.2006.01102.x](https://doi.org/10.1111/j.1462-2920.2006.01102.x)
- Vincent, F., and others. 2023. Viral infection switches the balance between bacterial and eukaryotic recyclers of organic matter during coccolithophore blooms. *Nat. Commun.* **14**: 510. doi:[10.1038/s41467-023-36049-3](https://doi.org/10.1038/s41467-023-36049-3)
- Vogt, M., M. Steinke, S. Turner, A. Paulino, M. Meyerhöfer, U. Riebesell, C. Le Quéré, and P. Liss. 2008a. Dynamics of dimethylsulphonio propionate and dimethylsulphide under different CO₂ concentrations during a mesocosm experiment. *Biogeosciences* **5**: 407–419. doi:[10.5194/bg-5-407-2008](https://doi.org/10.5194/bg-5-407-2008)
- Vogt, M., S. M. Vallina, and R. von Glasow. 2008b. New directions: Correspondence on “Enhancing the natural cycle to slow global warming”. *Atmos. Environ.* **42**: 4803–4809. doi:[10.1016/j.atmosenv.2008.04.005](https://doi.org/10.1016/j.atmosenv.2008.04.005)
- Wang, S., M. E. Maltrud, S. M. Burrows, S. M. Elliott, and P. Cameron-Smith. 2018. Impacts of shifts in phytoplankton community on clouds and climate via the sulfur cycle. *Global Biogeochem. Cycl.* **32**: 1005–1026. doi:[10.1029/2017gb005862](https://doi.org/10.1029/2017gb005862)
- Wolfe, G. V., M. Steinke, and G. O. Kirst. 1997. Grazing-activated chemical defence in a unicellular marine alga. *Nature* **387**: 894–897. doi:[10.1038/43168](https://doi.org/10.1038/43168)
- Yang, M., S. D. Archer, B. W. Blomquist, D. T. Ho, V. P. Lance, and R. J. Torres. 2013. Lagrangian evolution of DMS during the Southern Ocean gas exchange experiment: The effects of vertical mixing and biological community shift. *J. Geophys. Res. Oceans* **118**: 6774–6790. doi:[10.1002/2013JC009329](https://doi.org/10.1002/2013JC009329)

Acknowledgments

The authors thank all the team members of the AQUACOSM VIMS-Ehux project for setting up and conducting the mesocosm experiment, and all the scientists who developed the concepts used in this article. This research has received funding from the European Research Council (ERC) under the European Union's Horizon 2020 research and innovation program (grant agreement #834162, SUMMIT Advanced Grant to RS). This research was also supported by a grant from the Simons Foundation (599207, M.Gr.). The Institute of Marine Sciences (ICM—CSIC) is supported by a “Severo Ochoa” Centre of Excellence grant (CEX2019-000928-S) from the Spanish government. We acknowledge support of the publication fee by the CSIC Open Access Publication

Support Initiative through its Unit of Information Resources for Research (URICI).

Conflict of Interest

None declared.

Submitted 11 November 2022

Revised 17 May 2023

Accepted 11 November 2023

Associate editor: Jana Himmers